2^{nd} Flow Control Conference
28 Jun - 1 Jul 2004 / Portland, Oregon

AIAA-2004-2319

Aerodynamic Performance of Biological Airfoils

Abel Vargas[*] and Rajat Mittal[†]
The George Washington University, Washington, D.C., 20052

Experimental studies on static, non-flapping dragonfly wings have shown favorable aerodynamic performance at low Reynolds number (Re ≤ 10,000). High lift is hypothesized to arise from the dragonfly's pleated wing structure. A numerical study of flow past a modeled dragonfly wing section as well as its comparison to a corresponding profiled airfoil and a flat plate were conducted at Re = 10,000. The main focus of the current investigation was to determine the primary flow features and mechanisms that are responsible for the enhanced performance of these biological wing sections at these relatively low Reynolds numbers. A time-accurate Cartesian grid based Navier-Stokes immersed boundary solver was utilized in the current study. The numerical results indicate that the pleated airfoil at a zero degree angle-of-attack generates the least drag despite its unconventional shape. Additionally, a higher transitory lift is produced by the pleated airfoil at a five degree angle-of-attack when compared to the profiled airfoil.

Nomenclature

c = chord length
C_D = drag coefficient
C_{Ds} = shear drag coefficient
C_{Dp} = pressure drag coefficient
C_L = lift coefficient
C_{Ls} = shear lift coefficient
C_{Lp} = pressure lift coefficient
P = Pressure
Re = Reynolds number
τ = thickness
t = dimensionless time
t^* = time
u_i = x_i component of velocity
U_∞ = free stream velocity
x_i = Cartesian coordinates
α = angle of attack

I. Introduction

A number of insect species including locusts, dragonflies, and damselflies employ wings that are pleated along the chord. These ultra-light membranous insect wings support a variety of aerodynamic and inertial forces during flight. The pleated framework provides stiffening against spanwise bending[1,2]. The vein network within the wing also plays an important role to resist mechanical wear that the wings endure during flapping. The vein framework consists of longitudinal, cross, and secondary veins (Fig.1). The veins are both a supporting framework and conduits for the transmission of hemolymph, oxygen, and sensory information, plus they prevent rips from spreading across the membrane[3]. The longitudinal veins are the main veins extending from the base of the wing joint. Cross veins extend from the primary longitudinal veins, and in insects such as dragonflies, a network of finer secondary veins completes the venal structure. The cross-veins act as stiffeners, allowing the membrane to carry

---

[*] Graduate Research Assistant, Department of Mechanical and Aerospace Engineering, Suite T739, 801 22nd Street N.W., Academic Center, Washington D.C. 20052, AIAA Student Member.

[†] Associate Professor, Department of Mechanical and Aerospace Engineering, Suite T729, 801 22nd Street N.W., Academic Center, Washington, D.C. 20052, AIAA Senior Member.

web shearing forces as pure tension. The pleated wing is structurally stabilized primarily by the folded configurations, which increases flexural rigidity[4]. The secondary veins also play an essential role in the overall stability of the wing, as they reduce buckling and structural failure[5].

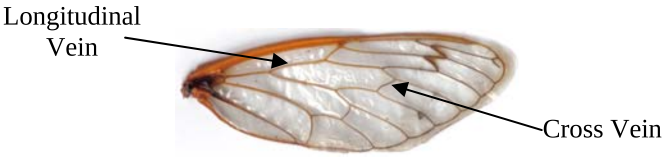

Figure 1. Vein framework of a Cicada (*Genus Magicicada)* wing illustrating the longitudinal and cross veins.

The cross section of a dragonfly wing (Fig. 2) does not resemble a typical engineered airfoil. Thus, it seems at the outset that such a pleated wing would have poor aerodynamic performance (low lift, extremely high drag) due to its un-conventional shape. However, experiments conducted on dragonfly wings in steady flow and gliding flight[6,7,8] and whole organism dragonflies in gliding flight[9] have led to surprising conclusions. It has been found that for flight conditions typical for a dragonfly, the pleated wing produces a higher lift when compared to technical airfoils. However, the underlying fluid dynamics is not completely understood and there are a number of different hypotheses put forth to explain the origin of this improved aerodynamic performance[1,7,8,10]. One hypothesis states that air flowing over the pleated airfoil becomes trapped between the folds where it either becomes stagnant or rotates slowly, resulting in the pleated wing acting as a streamlined airfoil[10], while a second hypothesis focuses on flow separation and reattachment. As the angle-of-attack is increased, the flow begins to separate from the leading edge forming a separation bubble that reattaches itself about 2/3 chord from the leading edge. Further increasing the angle-of-attack causes the reattached bubble to decrease in size resulting in increased lift[7]. Despite these different hypotheses, most studies agree that pleated wings work extremely well below the sub critical Reynolds number (Re < 70,000) and quite naturally point to the potential of employing such wings in micro-aerial vehicles.

Insects generate lift by different mechanisms in flight; some insects use the clap-and-fling mechanism[11] but most rely on the leading edge vortex (LEV) to generate lift. The dragonfly is no exception and it too must flap its hind and forewings to generate lift. The typical flapping frequency of dragonflies in forward flight is in the 25Hz-32Hz range[7,12]. However, dragonflies can be considered as gliders, because they commonly travel 40 chord lengths over one complete wing beat[7]. Furthermore, wing beat frequency declines considerably while the time spent gliding increases as the ambient temperature increases[13] and it has been hypothesized that dragonflies adopt this gliding mode to take advantage of convective cooling during hot weather. Gliding flight requires virtually no effort from the dragonfly, since it is able to relax the thoracic flight muscles which are responsible for heat generation[14]. Since gliding seems to be an integral part of a dragonfly's flight, it stands to reason that many of the features of the dragonfly wings, including the pleated structure, would have evolved to be advantageous during this flight mode. Consequently, there is hope that by understanding the flow physics associated with these wing features, better wing designs for micro-aerial vehicles can be developed.

Experimental measurements of the aerodynamic characteristics of dragonfly wing sections and their comparison to technical airfoils have been performed by Kesel[6]. However, a detailed examination of the unsteady flow, vorticity, and associated pressure field is difficult to achieve experimentally. In contrast, time-accurate, numerical simulations are well suited for this purpose and this forms the primary motivation for the current study. The objective of the current investigation is to describe a numerical study of flow past a modeled dragonfly wing section as well as its comparison to a corresponding profiled airfoil and a flat plate. Such an investigation will aid in determining the primary flow features and mechanisms that are responsible for the enhanced performance of these biological wing sections at relatively low Reynolds numbers.

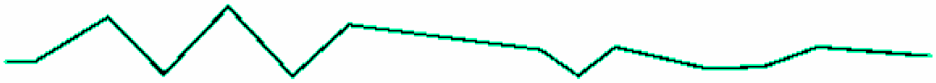

Figure 2. Typical cross-section of a dragonfly wing.

II. Numerical Methodology

The solver employs a time-dependent, conservative form of the incompressible Navier-Stokes equations discretized with a finite-difference approach. The incompressible Navier-Stokes equations written in tensor form are

$$\frac{\partial u_i}{\partial x_i} = 0$$
$$\frac{\partial u_i}{\partial t} + \frac{\partial (u_i u_j)}{\partial x_j} = -\frac{\partial P}{\partial x_i} + \frac{1}{\mathrm{Re}} \frac{\partial^2 u_i}{\partial x_j \partial x_j} \tag{1}$$

where the indices, i = 1, 2, 3, represent the x, y and z directions, respectively; and the velocity components are denoted by u_1, u_2, and u_3 corresponding to u, v, w respectively. The equations are non-dimensionalized with the appropriate length and velocity scales, in this case airfoil chord and freestream velocity respectively and Re is the corresponding Reynolds number. The Navier-Stokes equations are discretized using a cell-centered, non-staggered arrangement. In addition to the cell-center velocities, the face-center velocities are computed and used for calculating the volume flux of each cell. The advantage of separately computing the face-center velocities has been initially proposed by Zang et al.[15] and discussed in the context of the current method in Ye et al.[16] and Udaykumar et al.[17]. The equations are integrated in time using the fractional step method[18]. The first step calculates an intermediate velocity field from the momentum equations without the pressure gradient terms. The second step computes the pressure field by solving a Poisson equation. The pressure Poisson equation is computed with a solver based on PETSC libraries or a flexible and efficient multi-grid algorithm. The spatial terms are discretized with a second-order accurate central-difference scheme. The convective terms are discretized using an explicit Adams-Bashforth scheme, and the diffusion terms are discretized with an implicit Crank-Nicolson technique which eliminates the viscous stability constraint.

The solver employs a Cartesian grid method wherein flow past complex geometries[19,20] is simulated on non-body conformal Cartesian grids. The immersed boundary is constructed from a number of marker points. A ghost-cell approach[21] is implemented which incorporates the effect of the immersed boundary on the flow, while preserving second-order accuracy. Ghost-cells are cells whose centers lie inside the immersed body and have at least one neighboring cell which lies outside the immersed body. The remaining cells with centers inside the body that are not adjacent to the immersed boundary are marked as solid cells. Figure 3 shows the marker points, fluid cells, ghost cells, and solid cells for an immersed boundary on a Cartesian grid. A normal probe is extended from the ghost cell to the immersed boundary. The intersection of the normal probe to the immersed boundary is called the boundary intercept point. The normal probe is extended further into fluid to a point referred to as a probe tip. Four cell nodes which surround the probe tip are then identified and a bilinear interpolation is employed to calculate a value at the probe tip. The flow variables at the ghost cells are then computed by extrapolating values from the probe tip and boundary-intercept points. This process satisfies appropriate Dirichlet or Neumann's boundary conditions on the boundary intercept point and maintains second-order global as well as local spatial accuracy.

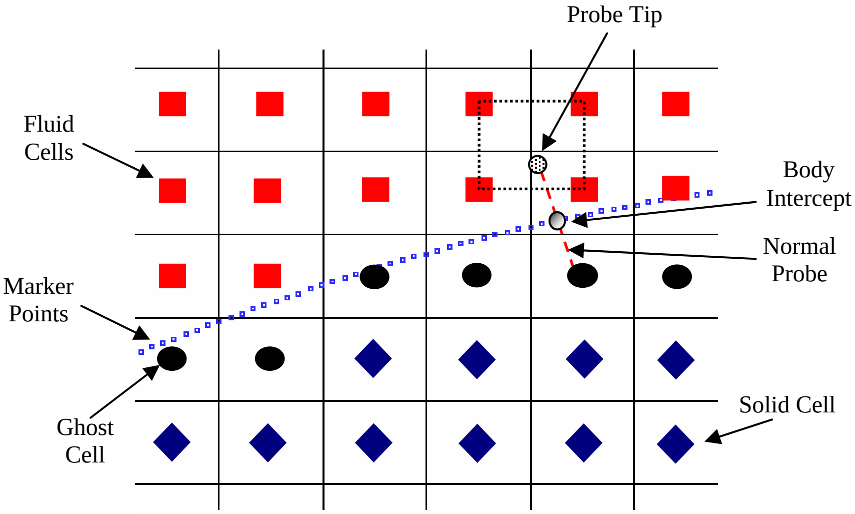

Figure 3. Schematic depicting the ghost-cell procedure.

A. Airfoil Shapes and Flow Configuration

The pleated geometry corresponds to the forewing of a dragonfly (*Aeshna cyanea*) acquired at the mid section of the wing which was digitally extracted from the paper of Kesel[6]. The specific profile chosen corresponds to "Profile 2" of Kesel[6]. For the purposes of the simulation, the sharp edges of the pleats were smoothened out without affecting the basic geometry of the pleats. A profiled airfoil was also constructed by fitting a spline through the local extrema of the dragonfly wing section as shown in the Fig. 4 (b). Finally, a flat plate airfoil similar to that of Kesel[6] was also included as a baseline case that would represent a flat wing without pleats. For comparison purposes, all length scales used in the experiments of Kesel[6] were incorporated in the design of the geometries. Figure 4 shows the cross section of the geometries used in the numerical study with a τ/c ratio of 7.531% for the pleated and profiled airfoil and a τ/c ratio of 3.342% for the flat plate, where τ is the thickness and c is the chord length.

The computational domain was chosen to be large enough so that the boundary effects on the flow development were negligible. A constant inflow velocity (U_∞) was imposed on the left boundary of the domain and the right boundary was set as an outflow boundary. The simulations for the pleated airfoil, profiled airfoil, and the flat plate, were carried out at 0.0 and 5.0 degree angles-of-attack at a chord-based Reynolds number of 10,000 which matched that of Kesel[6] and is a typical flow regime for dragonflies in flight. The results presented here have been produced on a dense 926x211 non-uniform Cartesian grid (Fig. 5), which was chosen to ensure that flow in the vicinity of the airfoil and the wake was well resolved.

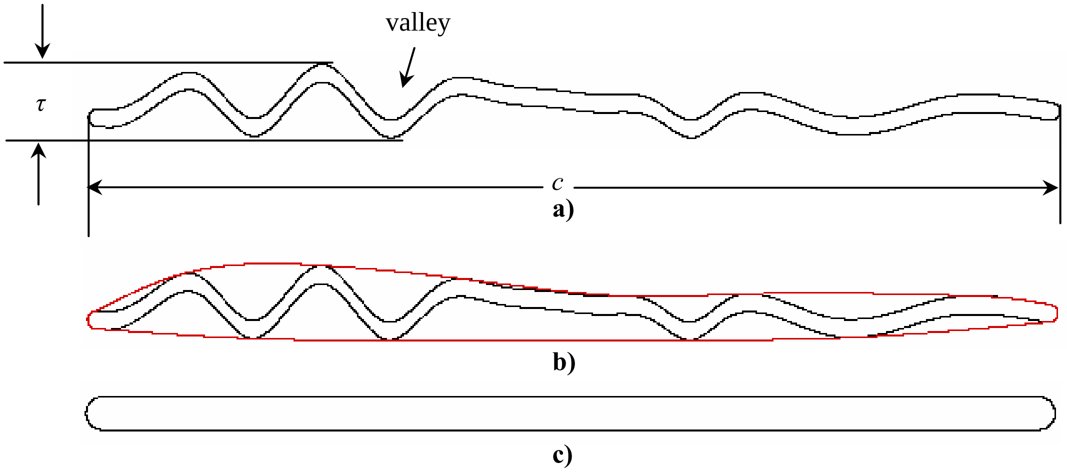

Figure 4. a) Pleated airfoil b) profiled airfoil with a τ/c = 7.531% and c) flat plate with τ/c = 3.342% used in the two-dimensional numerical simulation.

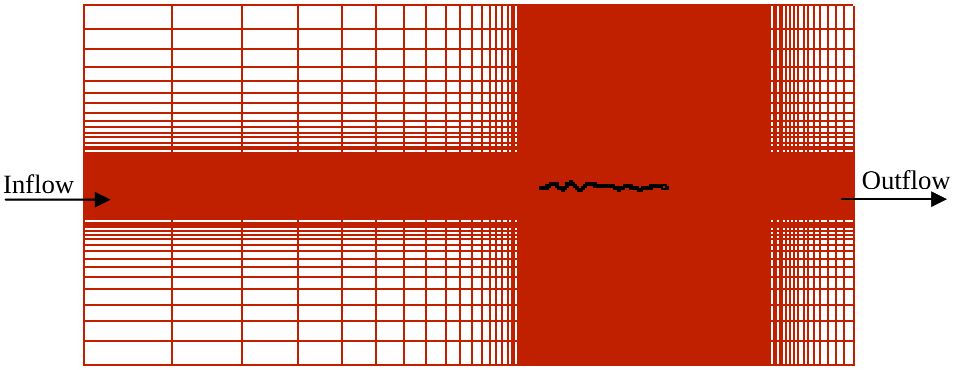

Figure 5. Non-uniform Cartesian grid (926 x 211) used in the numerical simulation.

III. Results

The following section discusses the aerodynamic performance of the pleated airfoil and its comparison to a profiled airfoil and a flat plate at 0.0 and 5.0 degree angles-of-attack. The simulations have been run for seven chord flow time units. Although this is adequate to obtain a statistically stationary state for the $\alpha = 0.0$ ° case, simulations for the 5.0 angle-of-attack case needs to be run longer in order to eliminate transients. However, a number of qualitative observations have been made from the preliminary data obtained from these simulations.

A. Angle of Attack = 0.0 °

Spanwise vorticity contour plots at a 0.0 degree angle-of-attack are shown in Fig. 6 at three different time instants. In these plots, red and blue contours represent counter-clockwise and clockwise vorticity respectively and a number of interesting observations can be made. First, the vorticity field for the pleated airfoil is significantly more complicated than that of the profiled airfoil, with clear evidence of flow separation and reattachment over the "valleys". Second, although both foils indicate the presence of Kármán vortex shedding in the wake, vortex shedding is also observed to occur over the lower surface of the pleated airfoil. Figure 7 clearly illustrates the presence of at least three circulation regions rotating in opposite direction at a non-dimensional time $t = t * U_\infty / c$ of 1.0 in the first valley on the suction surface. These separate recirculation regions are seen to merge over time and at t = 3.0, a large recirculation region dominates each valley in the pleated airfoil (Fig. 7). There is no indication of vortex shedding occurring over the valleys since the streamlines do not change from t = 2.0 to t = 6.0. The trapped vortex in each valley eventually forms the profile of a smoothened airfoil as demonstrated in Fig. 8, which is inline with the conclusions of Rees[10] who hypothesized that flow would become trapped inside the valleys.

Interestingly, the wake of the profiled airfoil is found to be quite different from that of the pleated airfoil. At first, the profiled airfoil shows evidence of Kármán vortex shedding in the near wake. However, as time proceeds, the location of vortex shedding moves farther downstream, so much that at a dimensionless time greater than 3.0, the flow is seen to leave the trailing edge smoothly. In contrast, the flat plate exhibits Kármán vortex shedding in the wake, which is responsible for the generation of oscillatory lift.

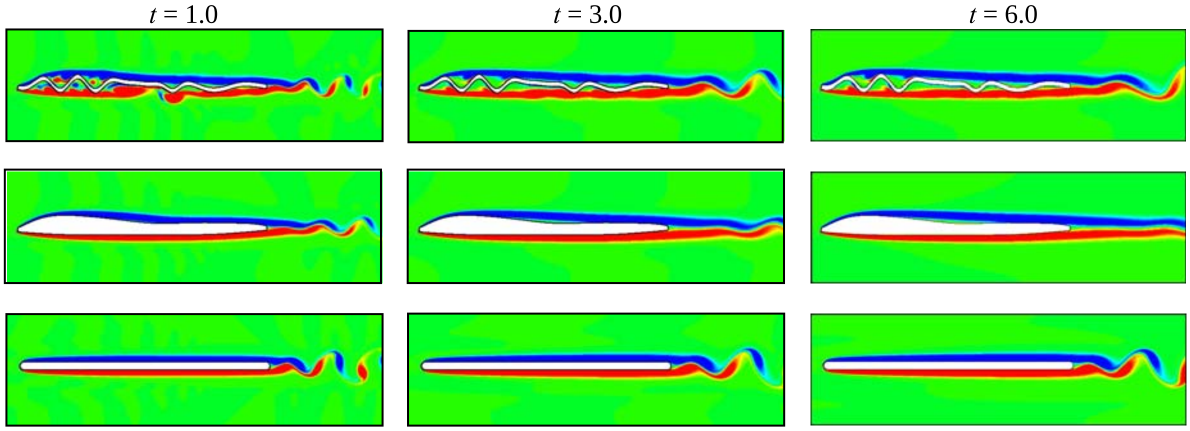

Figure 6. Vorticity contour plots at three non-dimensional time units at $\alpha = 0.0^{o}$.

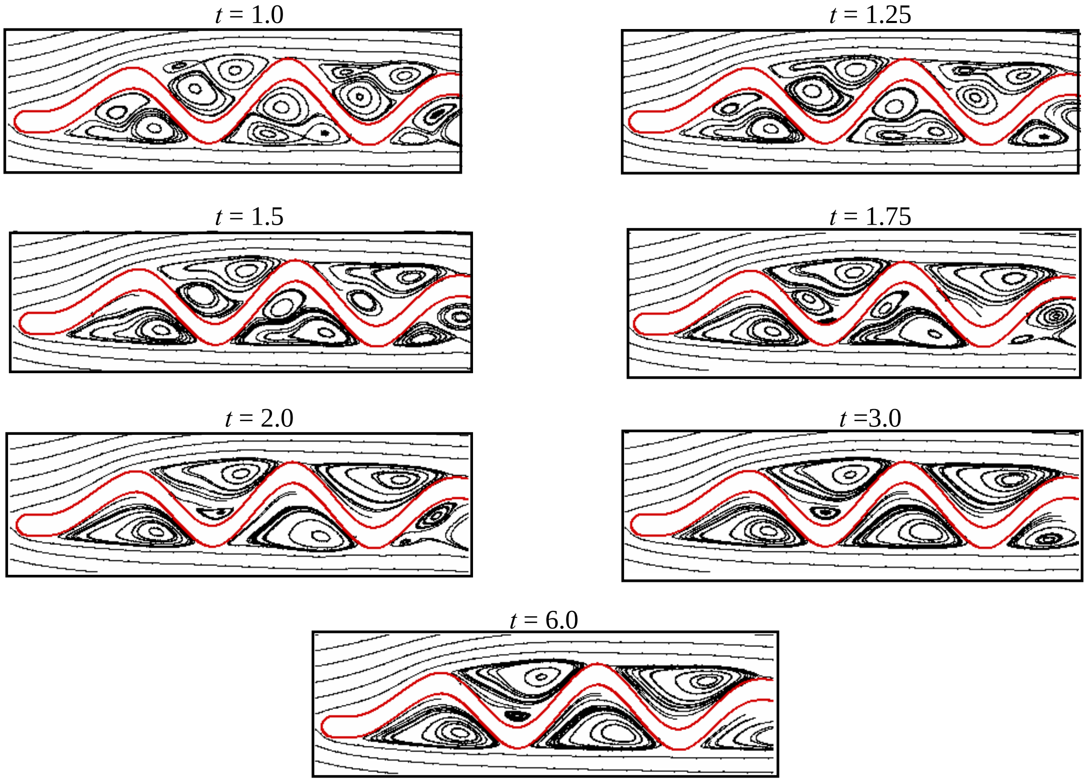

$t = 1.0$

$t = 1.25$

$t = 1.5$

$t = 1.75$

$t = 2.0$

$t = 3.0$

$t = 6.0$

Figure 7. Streamlines at different time units illustrating the circulation regions inside the valleys of the pleated airfoil at $\alpha = 0.0$ °.

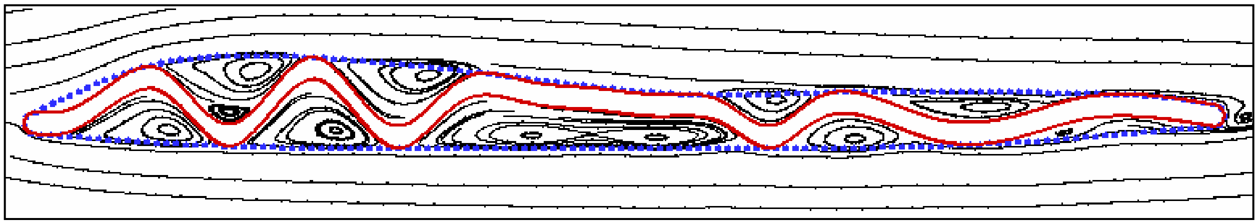

Figure 8. Streamlines generated by the pleated airfoil with the outline of the profiled airfoil superimposed.

The time histories of C_L and C_D for the pleated airfoil, profiled airfoil, and the flat plate are shown in Fig. 9. The pleated airfoil produces a sharp increase in lift at approximately 1.5 time units due to the shedding of a large vortex on the lower surface of the airfoil. The lift and drag coefficients for the pleated airfoil also show sustained oscillations which is due to the Kármán vortex shedding in the wake of the airfoil.

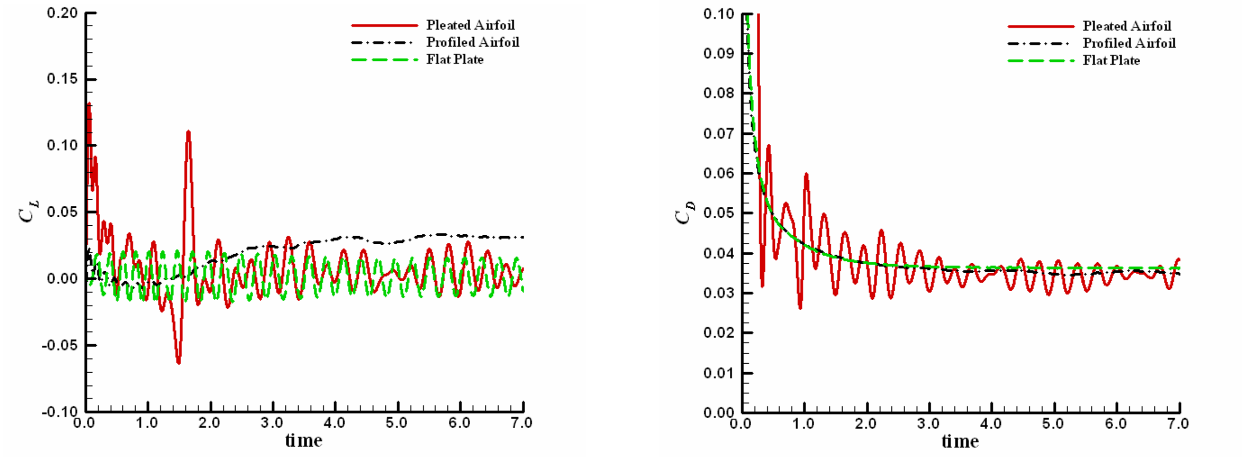

a) b)

Figure 9. Time history plots of a) C_L and b) C_D for geometries at $\alpha = 0.0$ ° angle-of-attack.

Time averaged force coefficients for the three geometries are compared to the published experimental results in Table 1. It should be noted that all time-averages have been restricted to a time period beyond 3.0 in order to eliminate transitory effects. The data in the Table 1 show that the profiled airfoil produces the largest lift and the value is about two times greater than the experimentally measured C_L. In contrast, the numerical C_L of the pleated airfoil is significantly less than that measured in the experiment, which demonstrates that the pleated airfoil section generates three times more lift than the smoothened airfoil. Thus, further investigation into this C_L discrepancy (especially in the pleated airfoil) is needed to verify the considerable difference in C_L.

Table 1. Numerical data compared to Kesel[6] obtained at $\alpha = 0.0$ °.

	NUMERICAL						EXPERIMENTAL	
	C_{Ls}	C_{Lp}	C_L	C_{Ds}	C_{Dp}	C_D	C_L	C_D
Pleated Airfoil	0.0012	0.0043	**0.0055**	0.0093	0.0252	**0.0345**	$0.053 \pm 3.71\text{x}10^{-4}$	$0.049 \pm 1.27\text{x}10^{-3}$
Profiled Airfoil	0.0017	0.0279	**0.0296**	0.0235	0.0118	**0.0353**	$0.016 \pm 1.12\text{x}10^{-4}$	$0.040 \pm 1.04\text{x}10^{-3}$
Flat Plate	-0.0001	0.0015	**0.0014**	0.0237	0.0127	**0.0364**	$0.022 \pm 1.98\text{x}10^{-4}$	$0.041 \pm 1.07\text{x}10^{-3}$

The numerical simulations yield a small but non-zero mean lift coefficient of 0.0014 for the flat-plate, which is most likely due to the statistical sampling error. Interestingly, the experiments measured a lift coefficient for the flat plate of about 0.022, which is higher than that measured for the profiled airfoil. The reason for this discrepancy in the experiment is not clear.

Comparison of the mean drag coefficients leads to some interesting observations. The numerical simulations show that the pleated airfoil, despite its highly corrugated shape, generates the least total drag. In order to better understand this behavior, the shear and pressure components of drag have also been tabulated in Table 1. Comparison of these components for the various cases shows that for both the profiled and flat plate airfoils, the shear drag is almost two-thirds of the total drag. In contrast, the shear drag for the pleated airfoil is only about one-fourth of the total drag. The lower shear drag is due to the reverse flow in the valleys, where the surface shear stress in these regions actually acts in the direction opposite to the flow. The pressure drag of the pleated airfoil is however about two times larger than that of the profiled and flat-plate airfoils. This is expected due to flow separation and reattachment that occurs over each valley of the pleated airfoil. Further analysis of the surface pressure distribution over the pleated airfoil is needed to confirm this hypothesis. Nevertheless, the numerical simulations clearly show the advantage of the pleated geometry at low Reynolds numbers. It is expected that at lower Reynolds numbers, where shear drag is even more dominant, the pleated airfoil will experience far less drag than the other two airfoils.

It should be pointed out that the numerical results are not entirely consistent with the experimental results of Kesel[6] in which the pleated wing section generates the most drag compared to the flat plate and the smoothed airfoil. The numerical drag of the profiled airfoil and the flat plate are however within about 11% of the experimental results of Kesel[6].

B. Angle of Attack = 5.0°

Vorticity contour plots for the three geometries at α = 5.0 ° are shown in Fig. 10. As in α = 0.0 ° case, the pleated airfoil at α = 5.0 ° exhibits flow separation and attachment in the valleys at t = 1.0. Also, there are at least two circulation regions present in each valley (Fig. 11), which then begin to merge as time advances to t = 2.0 units. At t = 3.0, a vortex is trapped in each convex valley, while vortex shedding appears to occur at the top valleys (Fig. 11). The flow then separates from the leading edge and reattaches itself to the top surface at a distance of 2/3 chord from the leading edge at t = 6.0 (Fig. 10). Similar reattachment for a different pleated airfoil was also observed by Newman et al.[7]. The profiled airfoil shows flow separation on the suction surface that is qualitatively quite similar to that observed for the pleated airfoil. This is somewhat surprising given the widely disparate airfoil shapes. For the flat plate, flow separation is more massive and occurs earlier in time.

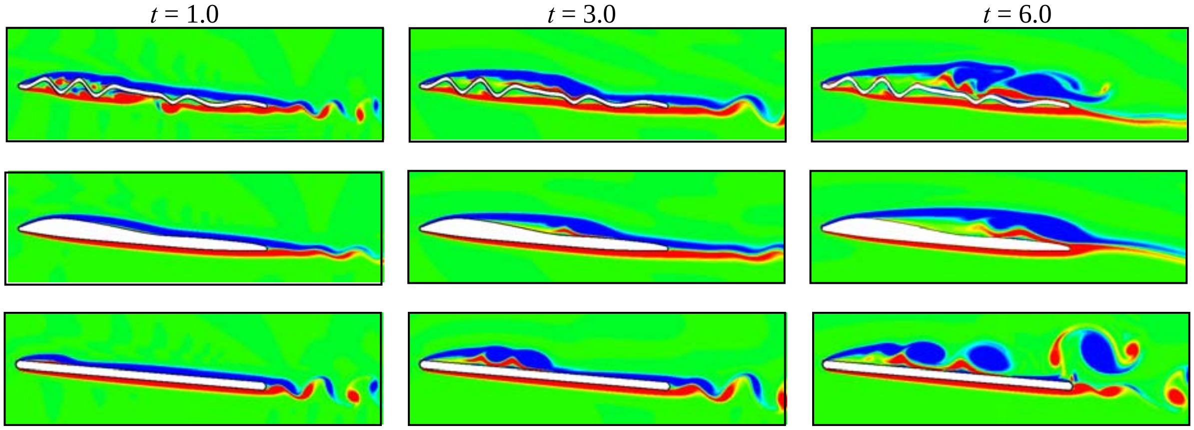
t = 1.0 t = 3.0 t = 6.0

Figure 10. Vorticity contour plots at three non-dimensional time units at α = 5.0 °.

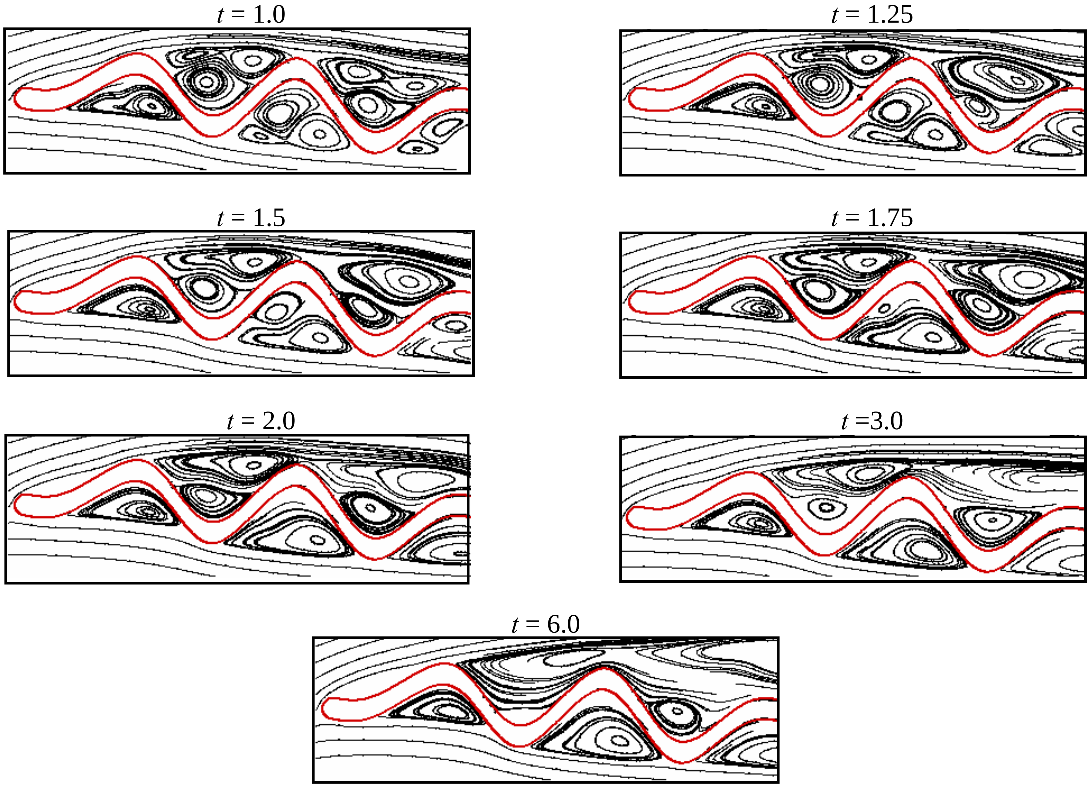
t = 1.0 t = 1.25

t = 1.5 t = 1.75

t = 2.0 t =3.0

t = 6.0

Figure 11. Streamlines at different time units illustrating the circulation regions inside the valleys of the pleated airfoil at α = 5.0 °.

The time history of C_L and C_D for these cases are shown in Fig. 12. The pleated airfoil reaches a maximum C_L = 1.10 at approximately t = 5.6, and maintains this value up to t = 6.6. This unit time corresponds to the reattachment of flow over the top surface where two clockwise vortices are present (Fig. 10). The profiled airfoil reaches its maximum value of C_L = 0.90 at about t = 5.0, but then a sudden decline in lift is observed due to the shedding of the top vortex occurring at t = 6.0 (Fig. 10). Thus, the pleated airfoil produces a 20% higher transitory lift peak than the profiled airfoil. This higher transitory lift would confer benefits during rapid maneuvering as would be required during escape or prey capture and needs further investigation. It is interesting to note that the flat plate generates the largest drag at α = 5.0° due to massive leading edge stall.

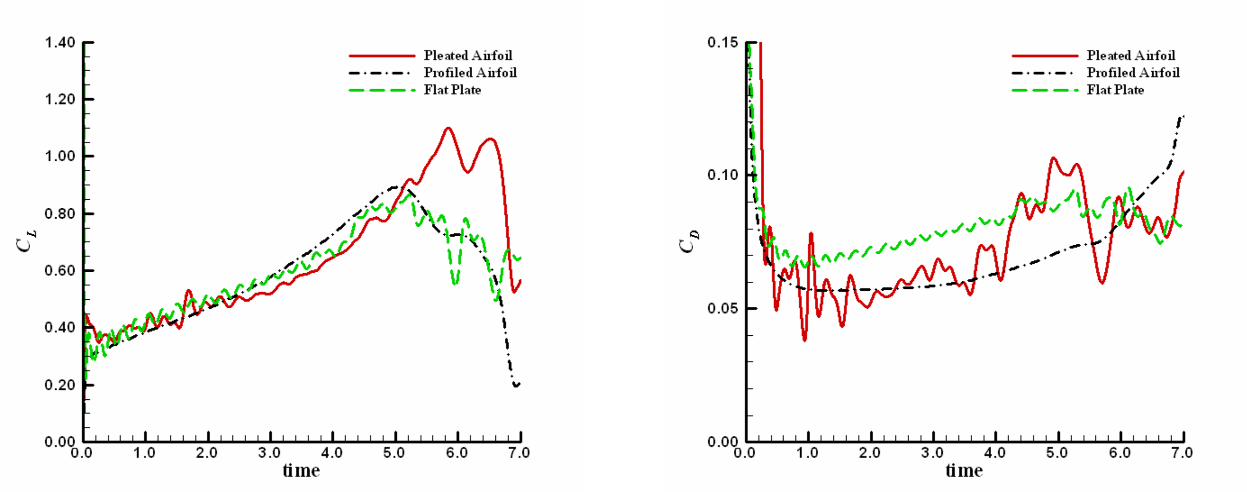

a) b)

Figure 12. Time history plots of a) C_L and b) C_D for geometries at α = 5.0 ° angle-of-attack

IV. Conclusions

Numerical simulations have been used to study the aerodynamic performance of a pleated airfoil and compare it to that of a profiled airfoil and a flat plate. Simulations confirm the notion that at zero angle of attack, recirculation regions inside the valleys of the pleats make the flow past the pleated airfoil look similar to that past a smoothened airfoil. The current investigation shows that the pleated structure tends to reduce the shear drag over the airfoil considerably whereas the pressure drag is higher than the corresponding profiled airfoil. Thus, it is clear that the pleated airfoil would have a greater advantage over the profiled airfoil at low Reynolds number where shear drag is dominant. For starting flow at a small angle-of-attack, the pleated airfoil shows a 20% increase in transitory lift compared to the profiled airfoil, and this could be beneficial during rapid maneuvering by the insect. All of these features could possibly be used to increase the performance of fixed-wing micro-aerial vehicles. Further analysis of the flow and pressure field is expected to yield greater insight into the flow physics underlying these observations.

Acknowledgments

The first author was supported by NASA-Harriett G. Jenkins Predoctoral Student Fellowship Grant. Support from the Office of Naval Research (Grant N00014-09-1-0897) is acknowledged.

References

[1] Hertel, H., *Structure, Form, Movement,* Reinhold, New York, 1966, pp 78-87.

[2] Newman, D. J. S. and Wootton, R., J., "An Approach to the Mechanics of Pleating in Dragonfly Wings," *Journal of Experimental Biology*, Vol. 125, 1986, pp. 361-372.

[3] Wootten, R. J., "Functional Morphology of Insect Wings," *Annual Review of Entomology,* Vol. 37, 1992, pp. 113-140.

[4] Rees, C. J. C., "Form and function in corrugated insect wings," *Nature,* Vol. 256, 1975a, pp.200-203.

[5] Kesel, A. B., Philippi, U. and Nachtigall, W., "Biomechanical Aspects of Insect Wings – An Analysis using the Finite Element Method," *Computers in Biology and Medicine,* Vol. 28, 1998, pp. 423–437.

[6] Kesel, A. B., "Aerodynamic Characteristics of Dragonfly Wing Sections Compared with Technical Aerofoil," *Journal of Experimental Biology*, Vol. 203, 2000, pp. 3125-3135.

[7] Newman, B. G., Savage, S. B., and Schouella, D., “Model Test on a Wing Section of a Aeschna Dragonfly”, *Scale Effects in Animal Locomotion,* edited by T. J. Pedley, London Academic Press, 1977, pp. 445-477.

[8] Okamato, M., Yasuda, K., and Azuma, A., “Aerodynamic Characteristics of the Wings and Body of a Dragonfly.” *Journal of Experimental Biology*. Vol. 199, 1996, pp. 281- 294.

[9] Wakeling, J. M. and Ellington, C. P**.**, **“**Dragonfly flight I. Gliding Flight and Steady-state Aerodynamic Forces,” *Journal of Experimental Biology,* Vol. 200, 1997, pp.543–556.

[10] Rees, C. J. C**.**, **“**Aerodynamic Properties of an Insect Wing Section and a Smooth Aerofoil Compared,” *Nature*, Vol. 258, 13 Nov. 1975b, pp 141-142.

[11] Weis-Fogh, T., “Quick Estimates of Flight Fitness in Hovering Animals, Including Novel Mechanisms for Lift Pproduction,” *Journal of Experimental Biology*, Vol. 59, 1973, pp. 169–230.

[12] Azuma, A. and Watanabe, T**.**, “Flight Performance of a Dragonfly,” *Journal of Experimental Biology,* Vol. 137**,** 1988, pp. 221–252.

[13] May, M. L., “Dependence of Flight Behavior and Heat Production on Air Temperature in the Green Darner Dragonfly *Anax junius* (Odonata: Aeshnidae),” *Journal of Experimental Biology,* Vol. 198, 1995, pp. 2385–2392.

[14] Nachtigall, W., *Insects in Flight – A glimpse behind the scenes in biophysical research,* London*,* Allen and Unwin, 1974.

[15] Zang, Y., Streett, R.L., and Koseff, J.R., , “A Non-Staggered Fractional Step Method for Time-Dependent Incompressible Navier-Stokes Equations in Curvilinear Coordinates,” *Journal of Computational Physics*, Vol. 114, 1994, pp. 18.

[16] Ye, T., Mittal, R., Udaykumar, H. S. and Shyy, W., “An Accurate Cartesian Grid Method for Viscous Incompressible Flows with Complex Immersed Boundaries,” *Journal of Computational Physics,* Vol. 156, 1999, pp. 209-240.

[17] Udaykumar, H. S., Mittal, R., Rampunggoon, P., and Khanna, A. “A Sharp Interface Cartesian Grid Method for Simulating Flows with Complex Moving Boundaries,” *Journal of Computational Physics,* Vol. 174, 2001, pp. 345-380.

[18] Chorin, A.J., “A Numerical Method for Solving Incompressible Viscous Flow Problems,” *Journal of Computational l Physics,* Vol. 2, 1967, pp. 12-26.

[19] Najjar, F. M., and Mittal, R., “Simulations of Complex Flows and Fluid-Structure Interaction Problems on Fixed Cartesian Grids,” *Proceedings of FEDSM’03 4TH ASME - JSME Joint Fluids Engineering Conference,* FEDSM 2003-45577, Honolulu, Hawaii, 2003.

[20] Mittal, R., Najjar, F.M., Byrganhalli, R., Seshadri, V., and Singh, H. “Simulation of Complex Biological Flows and Flow Control Problems on Cartesian Grids,” *Fifth International Conference on Advances in Fluid Mechanics*, Lisbon, Portugal, 2004.

[21] Ghias, R., Mittal, R., and Lund, T., S., “A Non-Body Conformal Grid Method for Simulation of Compressible Flows with Complex Immersed Boundaries,” *42nd AIAA Aerospace Sciences Meeting and Exhibit*, AIAA Paper 2004-0080, Reno, Nevada, 2004.